



QCD Induced Di-boson Production in Association with Two Jets at NLO QCD

Francisco Campanario^{a,1}, Matthias Kerner^{b,c}, Le Duc Ninh^{b,d}, Dieter Zeppenfeld^b

^aTheory Division, IFIC, University of Valencia-CSIC, E-46980 Paterna, Valencia, Spain

^bInstitute for Theoretical Physics, KIT, 76128 Karlsruhe, Germany

^cMax Planck Institute for Physics, Föhringer Ring 6, D-80805 München, Germany

^dHumboldt-Universität zu Berlin, Institut für Physik, Newtonstraße 15, D-12489 Berlin, Germany

Abstract

We discuss results for di-boson plus two jets production processes at the LHC at NLO QCD. Issues related to the scale choice are reviewed. We focus on the distributions of the invariant mass and rapidity separation of the two hardest jets and show, for $W^\pm\gamma jj$ and $Z\gamma jj$ production, how the contribution from the radiative decays of the massive gauge bosons can be significantly reduced.

Keywords: Collider Physics, multi-leg at NLO QCD, multi-boson production

1. Introduction

The experimental program at the LHC for measuring the di-boson in association with two jets production processes has started. Results for the same-sign $W^\pm W^\pm jj$ production process have already been reported by the ATLAS and CMS collaborations [1, 2]. They have presented first evidence for the electroweak (EW) induced production mechanism, thus, being able to distinguish it from the QCD induced one, considered to be a background, in the framework of vector boson scattering and quartic gauge coupling measurements.

Generally, the electroweak-induced production mechanism of order $\mathcal{O}(\alpha^4)$ (for on-shell vector boson production) can be classified into the t -channel vector-boson contributions, known for all the processes at NLO QCD [3–8] and other contributions, mainly, tri-boson production processes, with a subsequent hadronic decay from one of the vector bosons. The NLO QCD corrections are available via the VBFNLO program [9–11]. They make use of the matrix elements computed first for the tri-boson production processes including leptonic decays [12–17], and involve some approximations [18].

The NLO QCD corrections for the QCD-induced production mechanism of order $\mathcal{O}(\alpha_s^2\alpha^2)$ (for on-shell production) for all the di-boson production processes have been recently completed [19–29]. To this programme, including the leptonic decays of the vector bosons and all off-shell and spin-correlation effects, we have contributed with predictions for the $W^\pm Zjj$, $W^\pm\gamma jj$, $W^\pm W^\pm jj$, $ZZjj$ and $Z\gamma jj$ processes and the codes are available in the VBFNLO program package. We refer to them from now on by the on-shell production names for simplicity. In these proceedings, we briefly discuss them. A sketch of the calculations is given in Sect. 2. Numerical results are presented in Sect. 3. Finally, we conclude in Sect. 4

2. Computational Setup

To compute the di-boson production processes in association with two jets at NLO QCD, we follow the spinor-helicity amplitude method [30, 31] and the effective current approach, factorizing, in this way, the leptonic tensor containing the EW information from the QCD part. Two generic amplitudes contribute,

$$pp \rightarrow V_1 V_2 jj + X, \quad (1)$$

$$pp \rightarrow \hat{V} jj + X \quad (\text{absent in } W^\pm W^\pm jj). \quad (2)$$

¹Speaker. Prepared for the 37th International Conference on High Energy Physics (ICHEP 2014), 2-9 Jul 2014, Valencia, Spain.

In each process, the leptonic decays of the vector bosons are included via effective currents, e.g., for $ZZjj$ production, we have $V_i = Z/\gamma^* \rightarrow l_i^+ l_i^-$ ($i = 1, 2$) and $\hat{V} = Z/\gamma^* \rightarrow l_1^+ l_1^- l_2^+ l_2^-$. In this way, we take into account all off-shell effects and spin correlations. Since the leptonic tensors are globally set in our code, this procedure makes it straightforward to implement and check all the processes. For each process, we cross-check the LO and real emission corrections against Sherpa [32, 33] and agreement is found for integrated cross sections for all processes. Additionally, we have implemented two completely independent calculations for the processes (see Ref. [22]).

For processes involving photons in the final state, namely $W^\pm \gamma jj$ and $Z \gamma jj$, several technicalities arise: (1) a new set of scalar integrals not present in the off-shell photon case appears. We have checked the scalar-integral basis using two independent calculations; (2) to avoid the need of including photon fragmentation functions and to preserve the exact cancellation of the QCD infrared singularities, we use the photon isolation criterion à la Frixione [34]; (3) to optimize the Monte Carlo integration efficiency, the phase-space generator is divided into two separate regions generated as double EW boson production, $V_1 \gamma$ with subsequent decay of the V_1 vector boson, as well as \hat{V} production with three-body decays $\hat{W}(\hat{Z}) \rightarrow l\nu(l^+l^-, \bar{\nu}l)\gamma$ (see Ref. [28] for details).

At the partonic level, we classify the amplitudes into sub-processes with 4 quarks and those with 2 quarks and 2 gluons. The latter is absent in the $W^\pm W^\pm jj$ production process. This fact makes this channel very interesting since interference effects between the QCD- and the EW-production mechanisms are expected to be maximal.

Six-point rank-five one-loop tensor integrals appear in the 2-quark-2-gluon virtual amplitudes. For the $ZZjj$ production process, there are up to 42 six-point diagrams in the $gg \rightarrow u\bar{u}ZZ$ sub-amplitude. The 4-quark group is simpler with up to 24 generic hexagons for the subprocess $q_1 q_2 \rightarrow q_1 q_2 ZZ$. Since the kinematics are the same when replacing a Z boson for a photon, the hexagons can be re-used, using a cache system, in the other contributing sub-amplitudes, i.e., $Z\gamma^* jj$, $\gamma^* Zjj$ and $\gamma^* \gamma^* jj$.

Additionally, there are closed quark-loop diagrams. For the neutral production processes, we do not include closed-quark loops where the vector bosons or/and the Higgs boson are directly attached to the loop. This set of diagrams forms a gauge invariant subset and contributes at the few per mille level to the NLO results [21], and hence is negligible for all phenomenological purposes. The diagrams with a closed quark-loop and two or three

gluons attached to it are however included.

With our program, we obtain the NLO inclusive cross section with statistical error of 1% within 20 minutes ($W^\pm W^\pm jj$) to 4 hours ($Z\gamma jj$) on an Intel i7-3970X computer with one core and using the compiler Intel-iftor version 12.1.0. The distributions shown below are based on multiprocessor runs with a total statistical error of 0.03% at NLO.

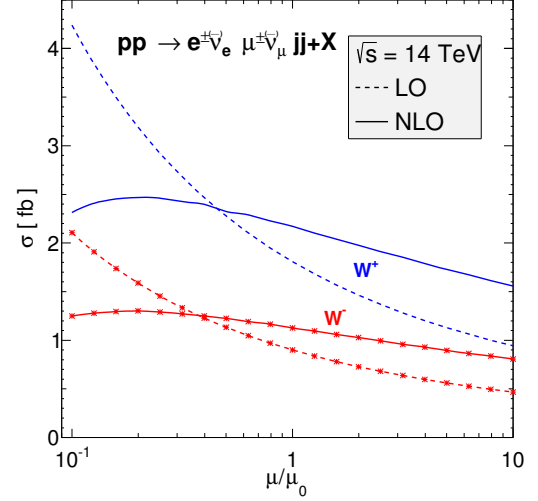


Figure 1: Scale dependence of the LO and NLO cross sections at the LHC. The curves with and without stars are for $W^- W^- jj$ and $W^+ W^+ jj$ productions, respectively. The cuts used are defined in the text.

3. Numerical Results

In the following, we present results for the LHC run at 14 TeV. We use the anti-kt algorithm [35] and consider jets that lie in the rapidity range $|y_{\text{jet}}| < 4.5$ and have transverse momenta $p_{T,\text{jet}} > 20$ GeV with a cone radius of $R=0.4$. For leptons, we use

$$p_{T,l} > 20 \text{ GeV} \quad |y_l| < 2.5 \quad R_{l(jl)} > 0.4, \quad (3)$$

and for processes with an on-shell photon,

$$p_{T,\gamma} > 30 \text{ GeV} \quad |y_\gamma| < 2.5 \quad R_{\gamma(jl)} > 0.7(0.4), \quad (4)$$

with the smooth isolation criterion à la Frixione [34]. With a cone radius of $\delta_0 = 0.7$, events are accepted if

$$\sum_{i \in \text{partons}} p_{T,i} \theta(R - R_{\gamma i}) \leq p_{T,\gamma} \frac{1 - \cos R}{1 - \cos \delta_0} \quad \forall R < \delta_0. \quad (5)$$

Finally, for processes with the W bosons, we impose that the missing transverse momentum associated with

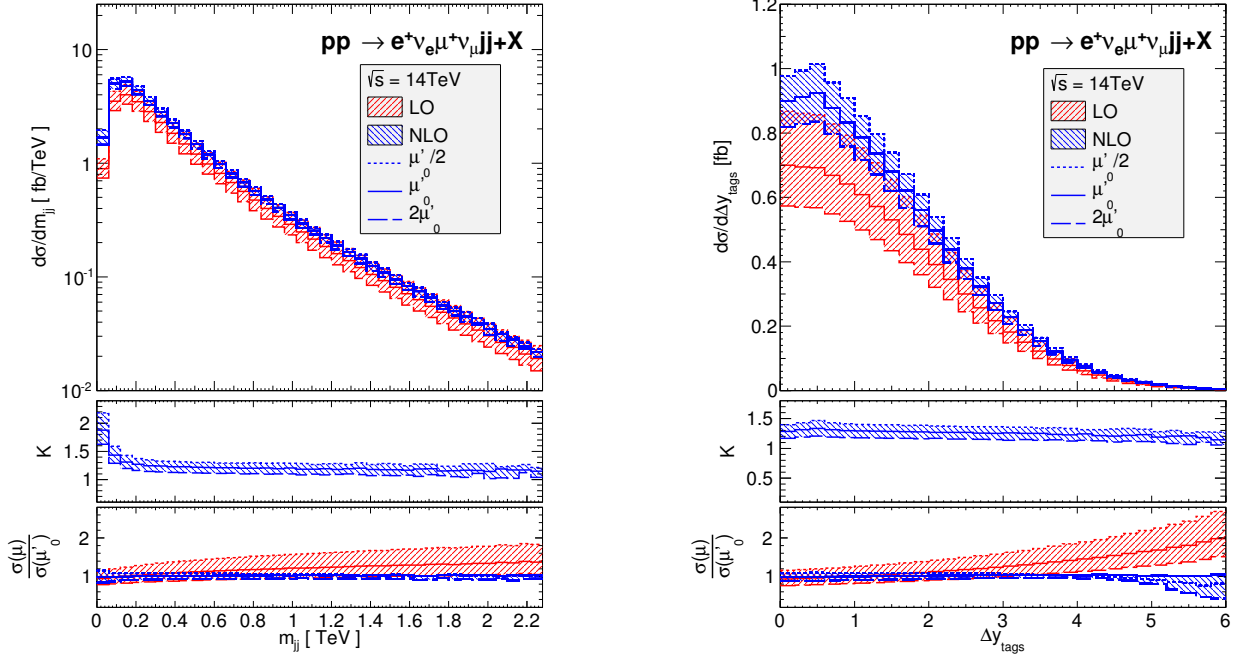


Figure 2: Differential cross sections for the QCD-induced channels at LO and NLO for the rapidity separation between the two tagging jets (right) and its invariant mass (left). The bands for the upper and middle panel describe $\mu'_0/2 \leq \mu_F = \mu_R \leq 2\mu'_0$ variations. The K -factor bands are due to the scale variations of the NLO results, with respect to $\sigma_{\text{LO}}(\mu'_0)$. The solid lines are for the central scale while the dotted and dashed lines correspond to $\mu'_0/2$ and $2\mu'_0$, respectively. Additional panels at the bottom show the ratios of differential cross sections with the scale μ_0 over the ones with μ'_0 at LO and NLO. The bands on these ratios show the scale variations $\mu_0/2 < \mu < 2\mu_0$ of the numerators while the denominators are calculated at the central scale.

the neutrinos is $p_T > 30$ GeV. For $W^\pm Z jj$ we have $m_{l^+l^-} > 15$ GeV in addition.

As EW input parameters, we use $M_W = 80.385$ GeV, $M_Z = 91.1876$ GeV and $G_F = 1.16637 \times 10^{-5}$ GeV $^{-2}$ and derive the mixing angle and the electromagnetic coupling from tree level relations. We use the MSTW2008 parton distribution functions [36] with $\alpha_S^{LO(NLO)}(M_Z) = 0.13939(0.12018)$. We assume a unit CKM matrix and consider all fermions massless, except the top quark with $m_t = 173.1$ GeV. The decay widths are fixed at $\Gamma_W = 2.09761$ GeV and at $\Gamma_Z = 2.508905$ GeV. We use the five flavor scheme. The top-quark contribution is decoupled from the running, but is explicitly included in the one-loop amplitudes.

We only consider equal renormalization and factorization scales in the following, but allow for three different choices of the central scales:

$$\mu_0 = \frac{1}{2} \left(\sum_{\text{partons}} p_{T,i} + \sum_{V_i} \sqrt{p_{T,V_i}^2 + m_{V_i}^2} \right),$$

$$\mu'_0 = \frac{1}{2} \left(\sum_{\text{jets}} p_{T,i} \exp |y_i - y_{12}| + \sum_{V_i} \sqrt{p_{T,V_i}^2 + m_{V_i}^2} \right),$$

$$\mu''_0 = \frac{1}{2} [E_T(jj) + E_T(VV)], \quad (6)$$

with $V_i \in (W, Z, \gamma)$. m_{V_i} denotes the invariant mass of the corresponding leptons ($m_{V_i} = 0$ for on-shell photons) and $y_{12} = (y_1 + y_2)/2$ the average rapidity of the two hardest (or tagging) jets, ordered by decreasing transverse momenta. $E_T(jj)$ and $E_T(VV)$ stand for the transverse energy of the two tagging jets and of the VV system, respectively. In the last two scale choices of Eq. (6), the first term interpolates between m_{jj} and $\sum p_{T,\text{jets}}$ for large and small $\Delta y_{jj} = |y_1 - y_2|$ values, characterizing the dynamics of these processes appropriately, as we will see below.

In Fig. 1, the renormalization and factorization scale variation plot is shown for $W^- W^- jj$ and $W^+ W^+ jj$ production. We observe a significant reduction in the scale dependence around μ_0 at NLO QCD. The uncertainties obtained by varying $\mu_{F,R}$ by a factor of 2 above and be-

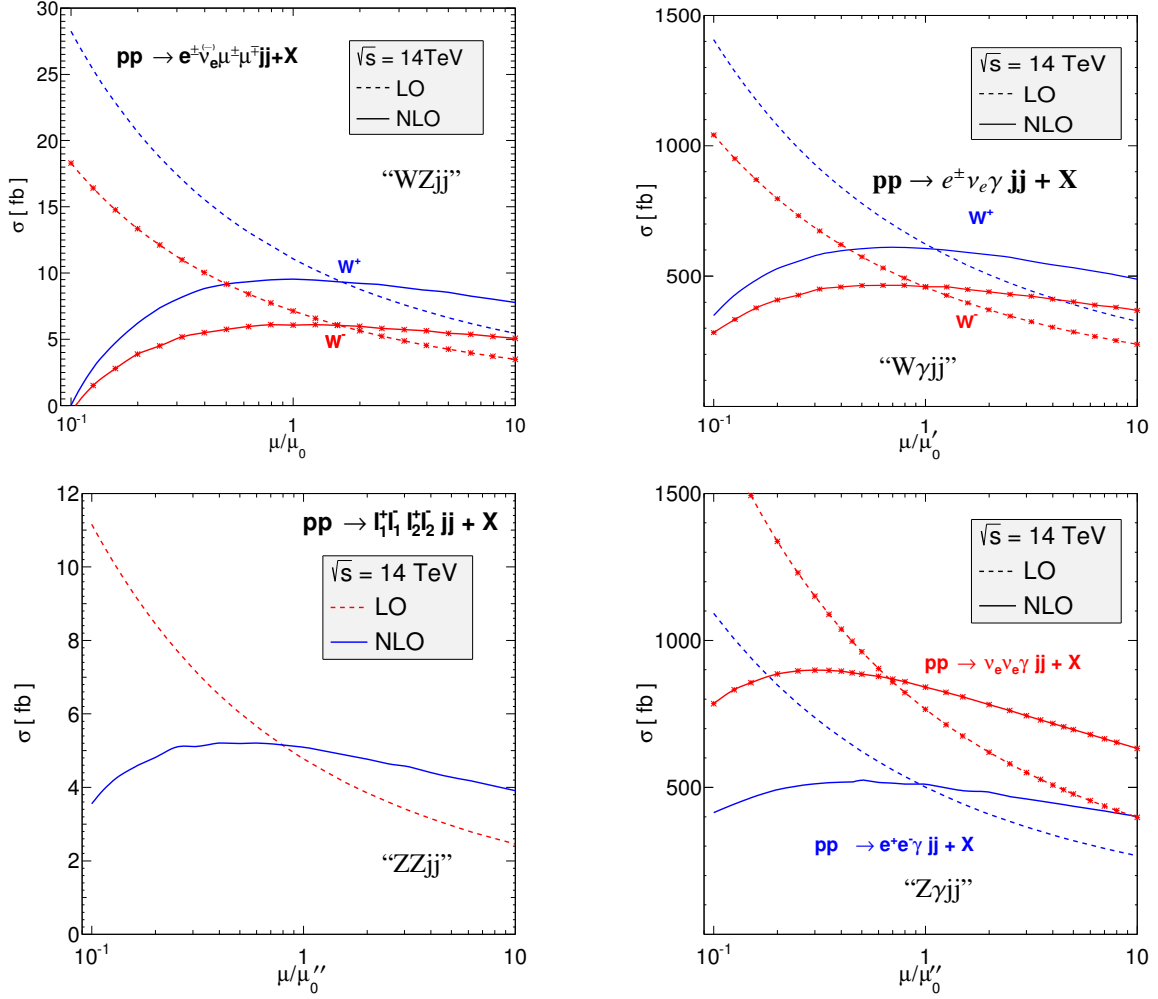


Figure 3: Scale dependence of the LO and NLO cross sections at the LHC. The central scales are defined in Eq. (6).

low the central value are 45% (45%) at LO and 16% (18%) at NLO for the W^+W^+ (W^-W^-) channel. If the two scales are varied separately (not shown), a small dependence on μ_F is observed, while the μ_R dependence is similar to the behavior shown in Fig. 1.

To illustrate the phase space dependence, we plot in Fig. 2, the differential distributions of the invariant mass (left) and the rapidity separation (right) for two different choices of the central scale. The upper and middle panel show the curves with respect to μ'_o . The middle panel shows the K-factor, defined as the ratio of the NLO to the LO predictions. Note the almost flat K-factor in the whole spectrum. This is not the case if the μ_0 scale is chosen as a central scale as can be inferred from the lower panels where the ratio of the cross sections for the two scales are plotted. Note the large differences of order of 2 at the LO for the Δy_{jj}

distribution. This shows the sensitivity of the LO predictions to different scale choices and the relevance of the NLO predictions to stabilize the results. The failure of the μ_0 scale to describe the dynamics can be understood in the following way: The invariant mass m_{jj} of the two leading jets rapidly increases at large rapidity separation Δy_{jj} , even though the tagging jets are mainly produced with low p_T , as can be seen from $m_{jj}^2 \approx 2p_{T,j1}p_{T,j2}[\cosh(y_{j1} - y_{j2}) - \cos(\phi_{j1} - \phi_{j2})]$. Note the exponential growth of m_{jj} with Δy . The low value of $p_{T,j2}$ acts as a veto for further (central) jet activity, resulting in large QCD uncertainties.

In Fig. 3 we show the scale uncertainties for $W^\pm Zjj$ and $W^\pm \gamma jj$ in the upper row and for $ZZjj$ and $Z\gamma jj$ in the lower row. The reduction of the scale uncertainties is similar and significant in all the production processes going from 40% at LO to below 10% at

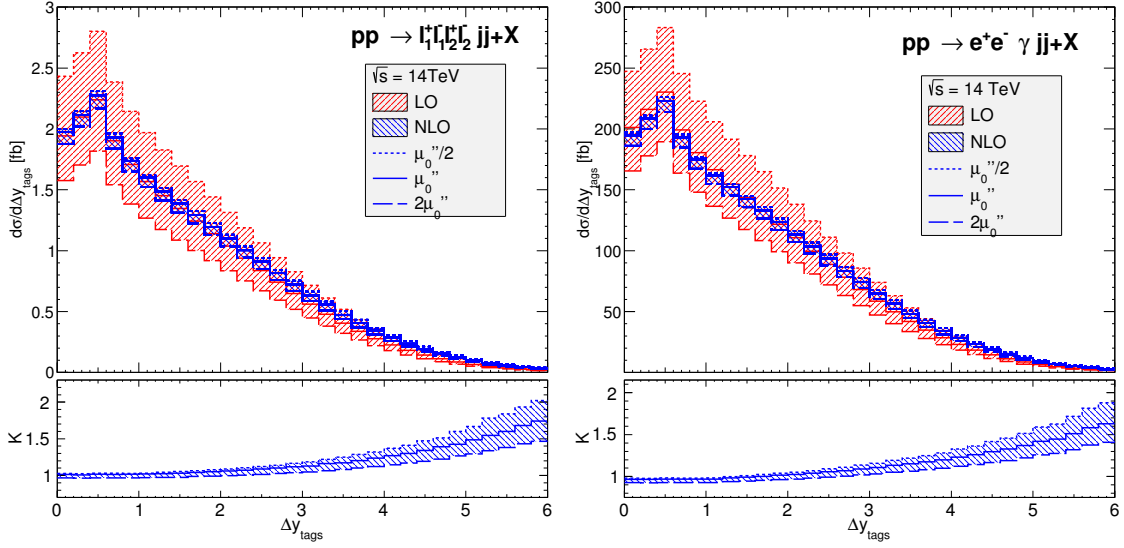


Figure 4: Differential cross sections for the QCD-induced channels at LO and NLO for the rapidity separation between the two tagging jets for the $ZZjj$ (left) and the $Z\gamma jj$ (right) production processes. More details in Fig. 2.

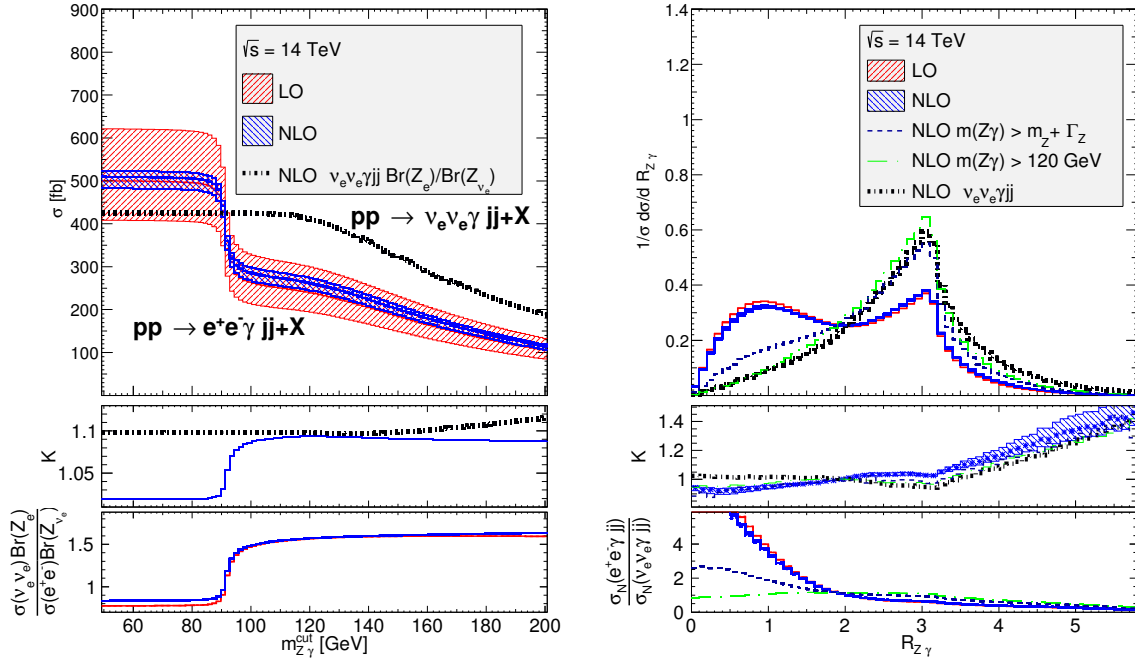


Figure 5: Left: Cross section for different values of the reconstructed $Z\gamma$ invariant mass cut. μ_0'' is chosen as a central scale. The neutrino curve is multiplied by the ratio of the charge-lepton versus neutrino branching ratios. The middle panel shows the K-factor and the lower the ratios of the modified neutrino cross section versus the LO and NLO electron cross sections. Right: Normalized differential distributions of the rapidity-azimuthal angle separation $R_{Z\gamma}$ for different values of the $m_{Z\gamma}^{cut}$ cut. The middle and lower panels show the differential K-factor plots and the ratios of the normalized electron versus neutrino pair production channels.

NLO. In Fig. 4, the differential distribution for the rapidity difference of the two tagging jets is plotted for

the $ZZjj$ and $Z\gamma jj$ production processes. Note the similar phase space dependence. Here, the large K-factors in

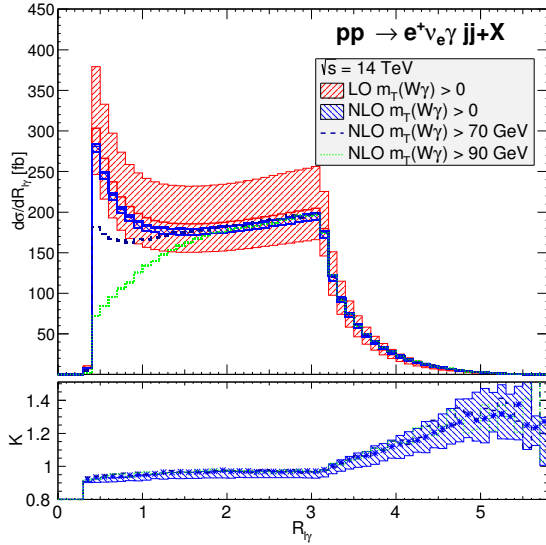


Figure 6: Differential cross sections of rapidity-azimuthal angle separation for different values of the transverse cluster energy of the $W\gamma$ system $m_{T,(W\gamma)}$. μ'_0 as a central scale is chosen.

the tails might indicate that the central scale at LO is too high. NLO curves for our three different scale choices (not shown) are within the scale uncertainty band of a variation by a factor 2, highlighting the relevance of the NLO predictions.

Next, we investigate the radiative photon emission off the charged leptons in $Z\gamma jj$ and $W^\pm\gamma jj$ production. This radiative decay represents a simple QED effect, which diminishes the sensitivity to anomalous couplings. Radiative decays dominate in the phase-space region where the reconstructed invariant mass of the $Z\gamma$ ($W\gamma$) system is close to the Z (W) mass. Thus, imposing a cut on $M_{Z\gamma}$ ($M_{T,W\gamma}$) slightly above the Z (W) mass should remove these contributions. For $Z\gamma jj$ production, we can make use of the $pp \rightarrow \nu\bar{\nu}\gamma jj$ (“ $Z_\nu\gamma jj$ ”) channel, in which radiative decays are absent, to determine the optimum value of the cut. The integrated cross section for the “ $Z_\nu\gamma jj$ ” and “ $Z\gamma jj$ ” channels are plotted as functions of the $m_{Z\gamma}$ cut in the left panel of Fig. 5. The latter is normalized by the ratio of the charge-lepton over the neutrino branching ratio of the Z boson. In the bottom panels, the ratio of the renormalized neutrino cross section to the electron cross sections are plotted. Note the sharp decrease of the cross section around the Z peak, indicating that radiative decays are eliminated. In the middle panel, one observes that a cut around $m_{Z\gamma}^{\text{cut}} = 120 \text{ GeV}$ would be optimal – the K-factor of the charge-lepton case stabilizes and

equals the neutrino channel. This is corroborated in the right panel, where the normalized differential distributions of the reconstructed rapidity-azimuthal angle separation of the $Z\gamma$ system are plotted for the two channels. One observes in the K-factor panel that, for the curve with the $M_{Z\gamma} > 120 \text{ GeV}$ cut, both channels behave approximately equal up to values of around 3, where the different cuts applied to the leptons appear to have an effect.

For the $W^\pm\gamma jj$ production process, this comparison is not possible. In Ref. [26], we showed that a cut on the transverse cluster mass of the EW system of around 90 GeV completely removes the radiative photon emission off the charged leptons with a very mild reduction of the total cross section of around 15% (see Fig. 6).

4. Conclusions

In these proceedings, NLO QCD results for several di-boson plus two jets production processes at the LHC have been discussed. The NLO QCD corrections significantly reduce the scale uncertainties. Large corrections can occur in differential distributions. Different (reasonable) scale choices at NLO QCD agree well with each other. However, large differences show up if only LO predictions are used. These facts emphasize the necessity and the relevance of the NLO QCD theoretical predictions. We have also found efficient cuts which reduce the photon-radiated-off-lepton contributions for $W^\pm\gamma jj$ and $Z\gamma jj$ production. All the processes are or will be available in the public program VBFNLO.

5. Acknowledgments

FC acknowledges financial support by the IEF-Marie Curie program (PIEF-GA-2011-298960) and partial funding by the LHCPHENONET (PITN-GA-2010-264564) and by the MINECO (FPA2011-23596). MK was funded by the graduate program GRK 1694: “Elementary particle physics at highest energy and precision”. LDN and DZ are supported in part by the Deutsche Forschungsgemeinschaft via the Sonderforschungsbereich/Transregio SFB/TR-9 “Computational Particle Physics”.

References

- [1] G. Aad, et al., Evidence for Electroweak Production of $W^\pm W^\pm jj$ in pp Collisions at $\sqrt{s} = 8 \text{ TeV}$ with the ATLAS Detector [arXiv:1405.6241](#).
- [2] CMS-Collaboration, Vector boson scattering in a final state with two jets and two same-sign leptons, CMS-PAS-SMP-13-015.

- [3] B. Jager, C. Oleari, D. Zeppenfeld, Next-to-leading order QCD corrections to $W+W^-$ production via vector-boson fusion, *JHEP* 0607 (2006) 015. [arXiv:hep-ph/0603177](#), doi:10.1088/1126-6708/2006/07/015.
- [4] B. Jager, C. Oleari, D. Zeppenfeld, Next-to-leading order QCD corrections to Z boson pair production via vector-boson fusion, *Phys.Rev.* D73 (2006) 113006. [arXiv:hep-ph/0604200](#), doi:10.1103/PhysRevD.73.113006.
- [5] B. Jager, C. Oleari, D. Zeppenfeld, Next-to-leading order QCD corrections to W^+W^-jj and W^-W^-jj production via weak-boson fusion, *Phys.Rev.* D80 (2009) 034022. [arXiv:arXiv:0907.0580](#), doi:10.1103/PhysRevD.80.034022.
- [6] G. Bozzi, B. Jager, C. Oleari, D. Zeppenfeld, Next-to-leading order QCD corrections to $W+Z$ and $W-Z$ production via vector-boson fusion, *Phys.Rev.* D75 (2007) 073004. [arXiv:hep-ph/0701105](#), doi:10.1103/PhysRevD.75.073004.
- [7] A. Denner, L. Hosekova, S. Kallweit, NLO QCD corrections to W^+W^-jj production in vector-boson fusion at the LHC, *Phys.Rev.* D86 (2012) 114014. [arXiv:arXiv:1209.2389](#), doi:10.1103/PhysRevD.86.114014.
- [8] F. Campanario, N. Kaiser, D. Zeppenfeld, $W\gamma$ production in vector boson fusion at NLO in QCD, *Phys.Rev.* D89 (2014) 014009. [arXiv:1309.7259](#), doi:10.1103/PhysRevD.89.014009.
- [9] K. Arnold, M. Bahr, G. Bozzi, F. Campanario, C. Englert, et al., VBFNLO: A Parton level Monte Carlo for processes with electroweak bosons, *Comput.Phys.Commun.* 180 (2009) 1661–1670. [arXiv:arXiv:0811.4559](#), doi:10.1016/j.cpc.2009.03.006.
- [10] K. Arnold, J. Bellm, G. Bozzi, M. Brieg, F. Campanario, et al., VBFNLO: A Parton Level Monte Carlo for Processes with Electroweak Bosons – Manual for Version 2.5.0 [arXiv:1107.4038](#).
- [11] J. Baglio, J. Bellm, F. Campanario, B. Feigl, J. Frank, et al., Release Note - VBFNLO 2.7.0 [arXiv:1404.3940](#).
- [12] V. Hankele, D. Zeppenfeld, QCD corrections to hadronic WWZ production with leptonic decays, *Phys.Lett.* B661 (2008) 103–108. [arXiv:arXiv:0712.3544](#), doi:10.1016/j.physletb.2008.02.014.
- [13] F. Campanario, V. Hankele, C. Oleari, S. Prestel, D. Zeppenfeld, QCD corrections to charged triple vector boson production with leptonic decay, *Phys.Rev.* D78 (2008) 094012. [arXiv:arXiv:0809.0790](#), doi:10.1103/PhysRevD.78.094012.
- [14] G. Bozzi, F. Campanario, V. Hankele, D. Zeppenfeld, NLO QCD corrections to $W+W^-$ gamma and ZZ gamma production with leptonic decays, *Phys.Rev.* D81 (2010) 094030. [arXiv:arXiv:0911.0438](#), doi:10.1103/PhysRevD.81.094030.
- [15] G. Bozzi, F. Campanario, M. Rauch, H. Rzehak, D. Zeppenfeld, NLO QCD corrections to $W^\pm Z\gamma$ production with leptonic decays, *Phys.Lett.* B696 (2011) 380–385. [arXiv:arXiv:1011.2206](#), doi:10.1016/j.physletb.2010.12.051.
- [16] G. Bozzi, F. Campanario, M. Rauch, D. Zeppenfeld, $W^{+\gamma}\gamma$ production with leptonic decays at NLO QCD, *Phys.Rev.* D83 (2011) 114035. [arXiv:arXiv:1103.4613](#), doi:10.1103/PhysRevD.83.114035.
- [17] G. Bozzi, F. Campanario, M. Rauch, D. Zeppenfeld, $Z\gamma\gamma$ production with leptonic decays and triple photon production at NLO QCD, *Phys.Rev.* D84 (2011) 074028. [arXiv:arXiv:1107.3149](#), doi:10.1103/PhysRevD.84.074028.
- [18] B. Feigl, Electroweak Processes in the Standard Model and Beyond: Backgrounds to Higgs Physics and Semileptonic Decay Modes.
- [19] T. Melia, K. Melnikov, R. Rontsch, G. Zanderighi, Next-to-leading order QCD predictions for W^+W^-jj production at the LHC, *JHEP* 1012 (2010) 053. [arXiv:arXiv:1007.5313](#), doi:10.1007/JHEP12(2010)053.
- [20] T. Melia, K. Melnikov, R. Rontsch, G. Zanderighi, NLO QCD corrections for W^+W^- pair production in association with two jets at hadron colliders, *Phys.Rev.* D83 (2011) 114043. [arXiv:arXiv:1104.2327](#), doi:10.1103/PhysRevD.83.114043.
- [21] N. Greiner, G. Heinrich, P. Mastrolia, G. Ossola, T. Reiter, et al., NLO QCD corrections to the production of W^+W^- plus two jets at the LHC, *Phys.Lett.* B713 (2012) 277–283. [arXiv:arXiv:1202.6004](#), doi:10.1016/j.physletb.2012.06.027.
- [22] F. Campanario, M. Kerner, L. D. Ninh, D. Zeppenfeld, WZ production in association with two jets at NLO in QCD, *Phys. Rev. Lett.* 111 (2013) 052003. [arXiv:arXiv:1305.1623](#), doi:10.1103/PhysRevLett.111.052003.
- [23] F. Campanario, M. Kerner, L. D. Ninh, D. Zeppenfeld, Next-to-leading order QCD corrections to W^+W^+ and W^-W^- production in association with two jets, *Phys.Rev.* D89 (2014) 054009. [arXiv:1311.6738](#), doi:10.1103/PhysRevD.89.054009.
- [24] T. Gehrmann, N. Greiner, G. Heinrich, Precise QCD predictions for the production of a photon pair in association with two jets, *Phys.Rev.Lett.* 111 (2013) 222002. [arXiv:1308.3660](#), doi:10.1103/PhysRevLett.111.222002.
- [25] S. Badger, A. Guffanti, V. Yundin, Next-to-leading order QCD corrections to di-photon production in association with up to three jets at the Large Hadron Collider, *JHEP* 1403 (2014) 122. [arXiv:1312.5927](#), doi:10.1007/JHEP03(2014)122.
- [26] F. Campanario, M. Kerner, L. D. Ninh, D. Zeppenfeld, Next-to-leading order QCD corrections to $W\gamma$ production in association with two jets, *Eur.Phys.J.* C74 (2014) 2882. [arXiv:1402.0505](#), doi:10.1140/epjc/s10052-014-2882-7.
- [27] Z. Bern, L. Dixon, F. Febres Cordero, S. Hoeche, H. Ita, et al., Next-to-Leading Order Gamma Gamma + 2-Jet Production at the LHC [arXiv:1402.4127](#).
- [28] F. Campanario, M. Kerner, L. D. Ninh, D. Zeppenfeld, Next-to-leading order QCD corrections to ZZ production in association with two jets, *JHEP* 1407 (2014) 148. [arXiv:1405.3972](#), doi:10.1007/JHEP07(2014)148.
- [29] F. Campanario, M. Kerner, L. D. Ninh, D. Zeppenfeld, $Z\gamma$ production in association with two jets at next-to-leading order QCD, *Eur.Phys.J.* C74 (9) (2014) 3085. [arXiv:1407.7857](#), doi:10.1140/epjc/s10052-014-3085-y.
- [30] K. Hagiwara, D. Zeppenfeld, Amplitudes for Multiparton Processes Involving a Current at e^+e^- , e^+p , and Hadron Colliders, *Nucl.Phys.* B313 (1989) 560. doi:10.1016/0550-3213(89)90397-0.
- [31] F. Campanario, Towards $pp \rightarrow VVjj$ at NLO QCD: Bosonic contributions to triple vector boson production plus jet, *JHEP* 1110 (2011) 070. [arXiv:arXiv:1105.0920](#), doi:10.1007/JHEP10(2011)070.
- [32] T. Gleisberg, S. Hoeche, F. Krauss, M. Schonherr, S. Schumann, et al., Event generation with SHERPA 1.1, *JHEP* 0902 (2009) 007. [arXiv:arXiv:0811.4622](#), doi:10.1088/1126-6708/2009/02/007.
- [33] T. Gleisberg, S. Hoeche, Comix, a new matrix element generator, *JHEP* 0812 (2008) 039. [arXiv:arXiv:0808.3674](#), doi:10.1088/1126-6708/2008/12/039.
- [34] S. Frixione, Isolated photons in perturbative QCD, *Phys.Lett.* B429 (1998) 369–374. [arXiv:hep-ph/9801442](#), doi:10.1016/S0370-2693(98)00454-7.
- [35] M. Cacciari, G. P. Salam, G. Soyez, The Anti-k(t) jet clustering algorithm, *JHEP* 0804 (2008) 063. [arXiv:arXiv:0802.1189](#), doi:10.1088/1126-6708/2008/04/063.
- [36] A. Martin, W. Stirling, R. Thorne, G. Watt, Parton distributions for the LHC, *Eur.Phys.J.* C63 (2009) 189–285. [arXiv:arXiv:0901.0002](#), doi:10.1140/epjc/s10052-009-1072-5.